

# Strong Coupling of Alfvén and Fast Modes in Compressible Relativistic Magnetohydrodynamic Turbulence in Magnetically-Dominated Plasmas

M. Takamoto,<sup>1\*</sup> and A. Lazarian<sup>2†</sup>

<sup>1</sup>*Department of Earth and Planetary Science, University of Tokyo, Tokyo 113-0033, Japan*

<sup>2</sup>*Department of Astronomy, University of Wisconsin, 475 North Charter Street, Madison, WI 53706, USA*

## ABSTRACT

In this paper, we report our detailed analysis of the new strong-coupling regime between Alfvén and fast modes in Poynting-dominated plasma turbulence, reported in our previous work Takamoto & Lazarian (2016), which is an important effect for many relativistic plasma phenomena, and calls for new theories of Poynting-dominated MHD turbulence. We performed numerical simulations of relativistic MHD turbulence in isothermal plasmas, and analyzed the ratio of fast to Alfvén mode energy. We found that the increase of the fast mode with the background  $\sigma$ -parameter can be observed even in isothermal plasma, showing that such a phenomena is universal in trans-Alfvénic turbulence in Poynting-dominated plasmas. To study the detailed energy conversion process, we also performed a series of simulations of decaying turbulence injecting pure Alfvén, fast, and slow modes, respectively, and investigated the development of the mode conversion from the each mode. We also found that the mode conversion between Alfvén and fast modes is nearly insensitive to the background temperature. Finally, we report a result of a simulation with initially fast mode dominated turbulence. It developed into a temporally strong-coupling regime, which is a strong evidence for the existence of our suggesting strong-coupling regime of fast and Alfvén modes. Our result suggests that the strong turbulence in Poynting-dominated plasma is very different from that in the non-relativistic plasma. It will also give an important guidance to studies of particle acceleration and non-thermal photon emission from Poynting-dominated plasma.

**Key words:** Turbulence — MHD — plasmas — methods:numerical.

## 1 INTRODUCTION

Turbulence plays an important role in many astrophysical phenomena. In particular, the effect of magnetic field is essential in many cases, and there has been a lot of studies on magnetohydrodynamic (MHD) turbulence. In non-relativistic case, it has been recognized that the coupling of each MHD characteristic mode is very weak, and they can be treated separately (Cho & Lazarian 2002, 2003), which provided with a vast amount of applicability of the critical-balance turbulence (Goldreich & Sridhar 1995) and Kolmogorov turbulence (Kolmogorov 1941) to various kinds of astrophysical phenomena. Comparing with non-relativistic work, much less attention has been given to relativistic turbulence (Thompson & Blaes 1998; Cho 2005; Inoue et al. 2011; Zrake & MacFadyen 2012, 2013; Radice & Rezzolla

2013; Cho & Lazarian 2014; Takamoto et al. 2015). Recently, Takamoto & Lazarian (2016) (TL16 in the following) has performed a mode decomposition of relativistic MHD turbulence, and reported that the coupling of each mode in relativistic MHD turbulence became stronger with increasing the background relativistic magnetization parameter  $\sigma$ , where  $\sigma$  is defined as  $\sigma \equiv B_0^2/4\pi\rho hc^2\gamma^2$  where  $B_0$  is the background magnetic field,  $\rho$  is the rest mass density,  $h$  is the specific enthalpy,  $c$  is the velocity of light, and  $\gamma$  is the Lorentz factor. However, TL16 assumed an adiabatic plasma which allowed increasing of the background temperature through thermalization of turbulence kinetic energy. In addition, it did not clarify the properties of the turbulence in the strong-coupling regime.

In this paper, we report our detailed analysis of the new strong-coupling regime between Alfvén and fast modes in Poynting-dominated plasma turbulence, reported in our previous work TL16. We performed numerical simulations of relativistic MHD turbulence in isothermal plasmas, and

\* E-mail: mtakamoto@eps.s.u-tokyo.ac.jp

† E-mail: alazarian@facstaff.wisc.edu

analyzed the ratio of fast to Alfvén mode energy. We also performed a simulation with initially fast mode dominated turbulence which allowed us to obtain temporally strong-coupling regime.

## 2 NUMERICAL SETUP

The plasma is modeled by the ideal RMHD approximation with the TM equation of state (Mignone et al. 2005) that allows us to simulate the relativistic perfect gas equation of state (Synge 1957) with less than 4 % error. The equations are updated using a numerical code originally developed by (Inoue et al. 2011) that combines the relativistic HLLD method (Mignone et al. 2009) in a conservative fashion and the constrained transport algorithm (Evans & Hawley 1988; Gardiner & Stone 2005). The initial background plasma is assumed to be uniform with magnetic field  $\mathbf{B}_0$ , density  $\rho_0$ , and temperature  $k_B T_0 / mc^2$  where  $k_B$  is the Boltzmann constant,  $T_0$  is the temperature,  $m$  is the particle mass. In the following, we set  $k_B = 1$  for simplicity. In our previous work TL16, a simple ideal RMHD plasma was considered which allowed its temperature variation from injected turbulence. Although we checked that our results were insensitive to the background temperature, it may have caused a suspicion that our results, indicating fast mode increasing in Poynting-dominated plasmas, was due to the background temperature increase. For this reason, an isothermal plasma is assumed in this work, that is, we solved the ideal RMHD equation every time step, and introduced an cooling in temperature whose timescale was 0.1 eddy-turnover time<sup>1</sup>.

In our work, the amount of Poynting energy in the plasma is measured by the following parameter  $\sigma$ , which is defined as

$$\sigma \equiv \frac{B_0^2}{4\pi\rho_0 h_0 c^2 \gamma_0^2}, \quad (1)$$

where  $h$  is the specific enthalpy determined by the TM equation of state, and  $\gamma$  is the Lorentz factor. The subscript 0 means the value of the background plasma. Originally, this parameter was defined by the ratio of the Poynting energy flux to particle energy flux; it reduces to the above form when considering the MHD state ( $\mathbf{E} = -\mathbf{v} \times \mathbf{B}$ ) with flowing perpendicular to the background magnetic field. Note that, in the case of RMHD turbulence, it is expected that the basic properties can be governed by  $\sigma$ -parameter and the temperature  $T$  because the RMHD characteristic velocities can be described by those 2-parameters and the angle between the propagation direction and the magnetic field (see also Equation (17)).

An isotropic turbulent velocity is injected at the initial time-step, simulating so-called *decaying turbulence*. Similar

<sup>1</sup> In our work, we did not use isothermal equation of state because of the numerical stability for solving trans-Alfvénic turbulence in high- $\sigma$  plasma which is usually very difficult to solve even when satisfying the conservation of energy. Note that this procedure in principle allows heating of the plasma for some regions, for example, expanding regions. It is, however, very rare because of the uniform injection of strong turbulence. A similar strategy was taken by Zrake & MacFadyen (2013).

to (Takamoto et al. 2015) and TL16, the turbulence is injected at large scales,  $l_{\text{inj}} = L/2, L/3, L/4$ , where  $L$  is the numerical box size, whose energy spectrum is assumed to be flat. We consider a cubic numerical domain that is divided by uniform meshes whose size is typically  $\Delta = L/512$ ; the higher resolutions,  $\Delta = L/1024$ , is used for obtaining the strong-coupling regime provided in Section 4.4.

## 3 MODE DECOMPOSITION OF RMHD TURBULENCE

### 3.1 Derivation of the Relativistic Displacement Vectors of RMHD Modes

There have already been a lot of references of linear perturbation of ideal RMHD equations. In this section, we just briefly introduce our derivation of the mode decomposition of the RMHD characteristic modes. In the following, we consider the analysis only in the fluid rest frame which is also used for our numerical simulations. The linear perturbation in the general frame was provided, for example, in (Anile 1990; Komissarov 1999; Balsara 2001; Antón et al. 2010). The ideal RMHD equations are given as:

$$\partial_t(\rho\gamma) + \nabla \cdot (\rho\gamma\mathbf{v}) = 0, \quad (2)$$

$$\partial_t[(\rho h + b^2)u^i u_j - b^i b_j] + \nabla_i[(\rho h + b^2)u^i u_j + (p_g + b^2/2)\delta_j^i - b^i b_j] = 0, \quad (3)$$

$$\partial_t \mathbf{B} = \nabla \times (\mathbf{v} \times \mathbf{B}), \quad \nabla \cdot \mathbf{B} = 0, \quad (4)$$

where  $i, j$  run from 1 to 3 following the Einstein rule,  $\delta_j^i$  is the identity matrix,  $u^\mu = \gamma(1, \mathbf{v})$  is the four velocity, and  $b^\mu = \gamma[\mathbf{v} \cdot \mathbf{B}, \mathbf{B}/\gamma^2 + (\mathbf{v} \cdot \mathbf{B})\mathbf{v}]$  is the covariant magnetic field which is the magnetic field in the fluid comoving frame. Note that the magnetic field is redefined as to absorb the coefficients, such as  $4\pi$  in the case of the Gauss unit. The perturbed variables are assumed to be written as:  $\delta Q \propto \exp[-i(\omega t + \mathbf{x} \cdot \mathbf{k})]$ , and the unperturbed variables are indicated by the subscript 0 as,  $Q_0$ . We assume an adiabatic equation of state,  $\delta p = c_s^2 h \delta \rho$  where  $c_s$  is the sound velocity depending on the background temperature  $T$  (Mignone et al. 2005). The perturbed equations of the above ones are given as:

$$-i\omega\delta\rho + i\mathbf{k} \cdot (\rho_0\delta\mathbf{v}) = 0, \quad (5)$$

$$-i\omega[(\rho_0 h_0 + B_0^2)\delta v^j - (\delta\mathbf{v} \cdot \mathbf{B}_0)B_0^j] + ik_i[(c_s^2 h_0 \delta\rho + \mathbf{B}_0 \cdot \delta\mathbf{B})\delta^{ij} - B_0^j \delta B^i - B_0^i \delta B^j] = 0, \quad (6)$$

$$-i\omega\delta\mathbf{B} = i\mathbf{k} \times (\delta\mathbf{v} \times \mathbf{B}_0), \quad i\mathbf{k} \cdot \delta\mathbf{B} = 0. \quad (7)$$

Similarly to the non-relativistic case, the above equations can be divided as:

$$-\omega\delta\rho/\rho_0 + k_x\delta v_x + k_y\delta v_y = 0, \quad (8)$$

$$-\omega\rho_0 h_0 \delta v^x + k_x(c_s^2 h_0 \delta\rho) = 0, \quad (9)$$

$$-\omega(\rho_0 h_0 + B_0^2)\delta v^y + k_y(c_s^2 h_0 \delta\rho + B_0 \delta B_x) - k_x B_0 \delta B^y = 0, \quad (10)$$

$$-\omega\delta B^y = B_0 k_x \delta v^y, \quad (11)$$

$$\delta B_x = -\frac{k_y \delta B_y}{k_x}, \quad (12)$$

and

$$-\omega(\rho_0 h_0 + B_0^2)\delta v^z - k_x B_0 \delta B^z = 0, \quad (13)$$

$$-\omega \delta B^z = B_0 k_x \delta v^z, \quad (14)$$

where the magnetic field is set in the  $x$ -direction, and the wave vector  $\mathbf{k}$  is assumed in the  $x$ - $y$  plane. It is well-known that the first set describes the fast and slow modes, and the second set describes the Alfvén mode. From the second set, it is clear that the Alfvén mode velocity can be obtained by projecting the velocity on the direction  $\mathbf{k} \times \mathbf{B}_0$ . The decomposition of fluid velocity onto fast and slow mode can be obtained by eliminating  $\delta\rho, \delta B_x, \delta B_y$  from Equations (8) to (12). From Equations (8) and (9), we obtain

$$\hat{\xi} \propto k_x \hat{k}_x + \left[ \frac{u^2}{c_s^2} k^2 - k_x^2 \right] \frac{1}{k_y^2} k_y \hat{k}_y, \quad (15)$$

where  $\hat{k}_i$  is a unit vector in the  $i$ -th direction. Similarly, using Equations (8), (10), (11) and (12), we obtain

$$\hat{\xi} \propto [u^2(1 + \sigma)k^2 - c_s^2 k_y^2 - \sigma k^2] \frac{1}{c_s^2 k_x^2} k_x \hat{k}_x + k_y \hat{k}_y. \quad (16)$$

Substituting the slow velocity  $u_{\text{slow}}$  in Equation (15), and the fast velocity  $u_{\text{fast}}$  in Equation (16), which, in the fluid comoving frame, are given as:

$$u_{\text{fast/slow}}^2 = \frac{1}{2} \left[ c_A^2 + \left( \cos^2 \theta + \frac{\sin^2 \theta}{1 + \sigma} \right) c_s^2 \pm \sqrt{\left\{ c_A^2 + \left( \cos^2 \theta + \frac{\sin^2 \theta}{1 + \sigma} \right) c_s^2 \right\}^2 - 4c_s^2 c_A^2 \cos^2 \theta} \right], \quad (17)$$

and the Equations (4) and (5) in TL16 are reproduced, which are also used for mode decomposition in the following.

### 3.2 Non-Relativistic Limit

In the non-relativistic limit, Equations (15) and (16) reduces to the Equation (1) and (2) in (Cho & Lazarian 2002) which are given as:

$$\hat{\xi}_{\text{slow}} \propto k_x \hat{k}_x + \frac{1 - \sqrt{D} - \beta/2}{1 + \sqrt{D} + \beta/2} \left[ \frac{k_x}{k_y} \right]^2 k_y \hat{k}_y, \quad (18)$$

$$\hat{\xi}_{\text{fast}} \propto \frac{1 - \sqrt{D} + \beta/2}{1 + \sqrt{D} - \beta/2} \left[ \frac{k_y}{k_x} \right]^2 k_x \hat{k}_x + k_y \hat{k}_y, \quad (19)$$

where  $D \equiv (1 + \beta/2)^2 - 2\beta \cos^2 \theta$  and  $\theta$  is the angle between magnetic field and wave vector:  $\mathbf{k} \cdot \mathbf{B}_0 = k B_0 \cos \theta = k_x B_0$ . After some calculations, the above equations can be rewritten as

$$\hat{\xi}_{\text{slow}} \propto k_x \hat{k}_x + \left( \frac{1 + \beta/2 - \sqrt{D}}{\beta \cos^2 \theta} - 1 \right) \left[ \frac{k_x}{k_y} \right]^2 k_y \hat{k}_y, \quad (20)$$

$$\hat{\xi}_{\text{fast}} \propto \left( \frac{(1 + \beta/2 + \sqrt{D}) - 2}{\beta \sin^2 \theta} - 1 \right) \left[ \frac{k_y}{k_x} \right]^2 k_x \hat{k}_x + k_y \hat{k}_y. \quad (21)$$

We start from the slow mode which can be obtained by substituting  $u = u_{\text{slow}}$  into Equation (15). It reduces to

$$\hat{\xi}_{\text{slow}} \propto k_x \hat{k}_x + \left[ \frac{u_{\text{slow}}^2}{c_s^2 \cos^2 \theta} - 1 \right] \left[ \frac{k_x}{k_y} \right]^2 k_y \hat{k}_y. \quad (22)$$

Cho & Lazarian (2002) considered an isothermal plasma, and the sound velocity can be rewritten as  $c_s^2 = c_A^2 \beta/2$ . In the non-relativistic case, the fast and slow velocity can be written as:

$$u_{\text{fast/slow}}^2 = \frac{c_A^2}{2} \left[ 1 + \frac{\beta}{2} \pm \sqrt{D} \right], \quad (23)$$

where  $+$  gives the fast velocity, and  $-$  the slow velocity. From these relations, it is clear that Equation (22) reduces to Equation (20). Next, in the non-relativistic limit, Equation (16) can be rewritten as

$$\hat{\xi}_{\text{fast}} \propto \left[ \frac{u_{\text{fast}}^2 - c_A^2}{c_s^2 \sin^2 \theta} - 1 \right] \left[ \frac{k_y}{k_x} \right]^2 k_x \hat{k}_x + k_y \hat{k}_y, \quad (24)$$

where  $u = u_{\text{fast}}$  and  $\sigma \simeq c_A^2$  are substituted. Similarly, it is clear that Equation (24) is equivalent to Equation (21).

### 3.3 Relativistic Corrections

In the strong magnetic field limit:  $\beta \rightarrow 0$ , the non-relativistic limit expressions, Equations (18) and (19), show that the slow mode displacement vector becomes parallel to the magnetic field, and the fast mode displacement vector becomes perpendicular to the magnetic field. In the following, we derive the displacement vectors in the relativistic plasma.

The corresponding limit in relativistic plasmas is the high- $\sigma$  limit, that is, the electromagnetic field energy is larger than the plasma rest mass energy. In the non-relativistic case, the sound velocity becomes negligibly small comparing with the Alfvén velocity in this limit. In the relativistic case, however, the sound velocity can be in general not so small comparing with the Alfvén velocity,  $0 \ll c_s < c_A \lesssim c$ , because the Alfvén velocity is bounded by the light velocity. This can occur when the background plasma temperature reaches around the rest mass energy,  $T \lesssim mc^2$ . Even 0.1% of the rest mass energy can make the sound velocity around 4% of the light velocity, which is considered to be realized in many high-energy astrophysical phenomena. In this limit,  $\sigma \gg 1$  and  $T/mc^2 \lesssim 1$ , the slow and fast mode velocities become

$$u_{\text{fast}}^2 \simeq c_A^2 + \frac{c_A^2 c_s^2 \sin^2 \theta}{\sigma(c_A^2 - c_s^2 \cos^2 \theta)}, \quad (25)$$

$$u_{\text{slow}}^2 \simeq c_s^2 \cos^2 \theta, \quad (26)$$

Substituting Equation (25) into Equation (16), the displacement vector becomes

$$\hat{\xi}_{\text{fast}} \propto \frac{c_s^2 \cos^2 \theta}{c_A^2 - c_s^2 \cos^2 \theta} \left[ \frac{k_y}{k_x} \right]^2 k_x \hat{k}_x + k_y \hat{k}_y. \quad (27)$$

Hence, the fast mode displacement vector has non-zero components parallel to the background magnetic field even in the high- $\sigma$  limit. Note that here we consider non-zero temperature which is the crucial difference from the force-free plasma discussed in (Thompson & Blaes 1998), and this makes our results more realistic because, in high- $\sigma$  plasmas, dissipation of small magnetic field fluctuations can result in thermal energy comparable to rest mass energy (Takamoto et al. 2014). Similarly, substituting Equation (26) into Equation (15), the slow mode displacement vector reduces to the same result as the non-relativistic case, that is, parallel to the background magnetic field direction. Note that in the high- $\sigma$  and low-temperature limit, Equations (25) and (26) reduce to

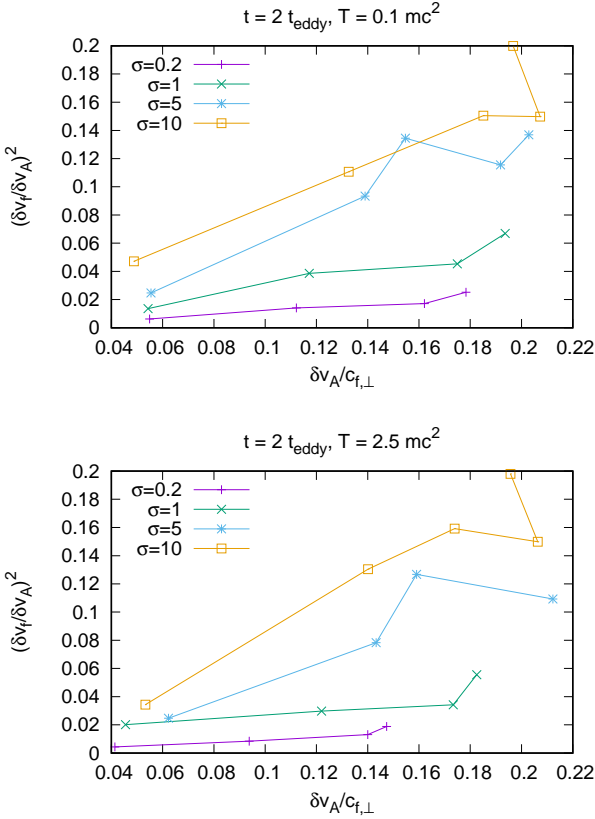


**Figure 1.** The ratio of fast to Alfvén mode power in terms of the non-relativistic fast Mach number which is measured using the Alfvén mode velocity at two eddy-turnover times. Top:  $T = 0.1mc^2$ , Bottom:  $T = 2.5mc^2$ .

$u_{\text{fast}}^2 \simeq c_A^2 + c_s^2 \sin^2 \theta / (1 + \sigma)$ , and  $u_{\text{slow}} \simeq c_s^2 \cos^2 \theta$ , which give the same result as the non-relativistic case.

#### 4 MODE COUPLING STUDY

In this section, we discuss the mode coupling between fast, slow, and Alfvén modes, and their dependence on the background  $\sigma$ -parameter.

##### 4.1 Ratio Between Compressible to Alfvén Modes

We performed numerical simulations of decaying turbulence. Similar to our previous work TL16, the Alfvénic mode velocity was injected initially, and we simulated the temporal evolution of the mode exchange in an isothermal plasma.

Figure 1 is the fast to Alfvén mode ratio at two eddy-turnover times where the eddy-turnover time is defined as  $t_{\text{eddy}} \equiv L/v_{\text{inj}}$ . The top panel is the results of cold plasma case with  $T/mc^2 = 0.1$ , and bottom panel is the results of hot plasma case with  $T/mc^2 = 2.5$ . Following (Cho & Lazarian 2002; Cho et al. 2002), the horizontal axis is the Alfvén mode velocity at two eddy-turnover times in the unit of the fast velocity in the direction perpendicular to

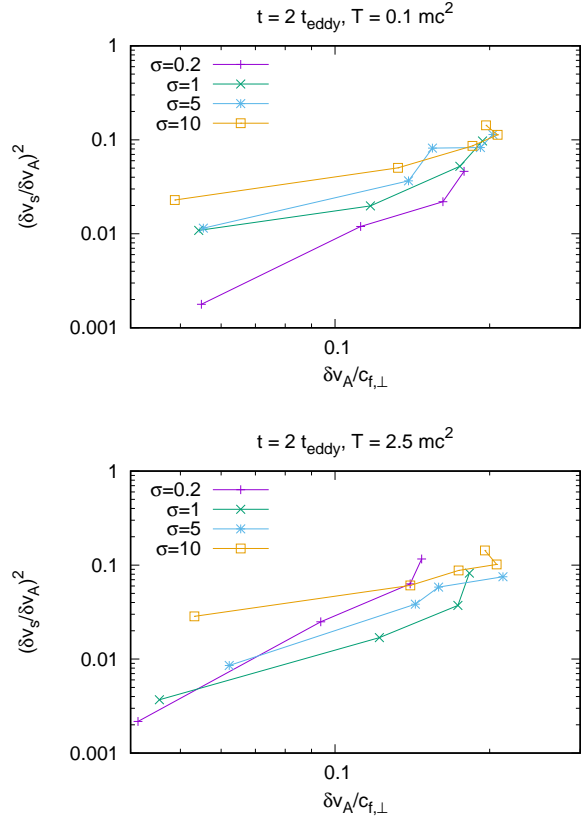


**Figure 2.** The ratio of slow to Alfvén mode power in terms of the non-relativistic fast Mach number which is measured using the Alfvén mode velocity at two eddy-turnover times. Top:  $T = 0.1mc^2$ , Bottom:  $T = 2.5mc^2$ .

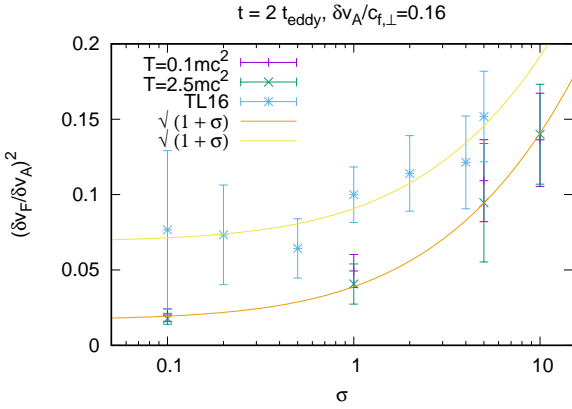
the background magnetic field<sup>2</sup>. Both show an increase of the ratio with the Alfvén mode velocity, and also with the background  $\sigma$  value, which is consistent with TL16.

Figure 2 is the slow to Alfvén mode ratio at two eddy-turnover times. The top panel is the results of cold plasma case with  $T/mc^2 = 0.1$ , and bottom panel is the results of hot plasma case with  $T/mc^2 = 2.5$ . Although it is difficult to find a clear dependence on the background  $\sigma$  parameter comparing with the fast to Alfvén mode power ratio, they also indicate that the ratio slightly increases with the Alfvén mode velocity<sup>3</sup>.

Figure 3 is a plot of the fast to Alfvén power ratio at  $\delta v_A / c_{f,\perp} = 0.16$  in terms of the background  $\sigma$  value. The purple and green points are the case of  $T = 0.1mc^2$  and

<sup>2</sup> Note that Equation (17) shows that the fast velocity has its maximum at the perpendicular direction to the background magnetic field. We use this maximum value for the unit of the injection velocity, which provides with a better correlation to the ratio of fast to Alfvén power.

<sup>3</sup> Note that both Figures 1 and 2 show decrease of Alfvén mode velocity in the case of  $\sigma = 10$ . This is because the trans-Alfvénic injection velocity,  $\lesssim 0.6c_A$ , induced a stronger non-linear effects, such as formation of shocks. This would convert more Alfvén mode energy into compressible modes one, resulting in reducing Alfvén mode velocity with increasing the compressible mode velocity.



**Figure 3.**  $\sigma$ -dependence of fast to Alfvén mode power ratio. TL16 means the adiabatic case studied in TL16.

$T = 2.5mc^2$ , respectively. They indicate that both cases can be fitted by a line:

$$(\delta v_F / \delta v_A)^2 \simeq A \sqrt{1 + \sigma} (\delta v_A / c_{f,\perp}), \quad (28)$$

where  $A$  is a parameter independent of background temperature indicated in Figure 3. The blue points are in the adiabatic gas case studied in our previous work TL16. It shows that both adiabatic and isothermal plasma turbulence show the same dependence on the  $\sigma$  value, proportional to  $\sqrt{1 + \sigma}^4$ . However, in the adiabatic case the ratio of fast to Alfvén power becomes clearly larger than that in the isothermal cases. We consider that this is because the present prescription of the cooling process breaks the conservation of the total energy, and some amount of the initial Alfvén mode energy was not converted into fast mode but disappeared from the system through the cooling. It also indicates that the physics of the non-linear coupling responsible for the mode conversion does not depend on whether the background plasma is adiabatic or not.

## 4.2 A Theoretical Consideration

In this section, we discuss a theoretical consideration of generation of compressible modes by Alfvén mode in high- $\sigma$  plasma using quasi-linear treatment. In the non-relativistic case, the displacement vector of each MHD mode velocity in low- $\beta$  plasma completely decouples as (Cho & Lazarian 2002):

$$\delta \mathbf{v}_A \propto \mathbf{e}_z, \quad \delta \mathbf{v}_F \propto \mathbf{e}_y, \quad \delta \mathbf{v}_S \propto \mathbf{e}_x, \quad (29)$$

where the same coordinate is selected as in Section 3. The magnetic field of these modes can be written as:

$$\delta \mathbf{B}_A = -\frac{B_0 \delta v_A}{c_A} \mathbf{e}_z, \quad \delta \mathbf{B}_F = \frac{B_0 \delta v_F}{c_A} [-k_x \mathbf{e}_y + k_y \mathbf{e}_x], \quad \delta \mathbf{B}_S = 0. \quad (30)$$

<sup>4</sup> Note that Figure 3 also plots error bars. These result from the fluctuation of each  $\sigma$ -value's curve in Figure 1 and 2 which reflects the statistical fluctuations of initial velocity field. This shows that the effect of fluctuation of initial condition increases with the background  $\sigma$ -parameter, describing a stronger generation of the compressible modes by the pressure gradient force as described in Equation (32), resulting in strong temporal fluctuations.

This shows that magnetic field of each mode also completely decouples. In the non-relativistic MHD case, the 2nd-order coupling was obtained assuming so called *weak turbulence approximation* (Kuznetsov 2001; Chandran 2005). It is found that the interaction between Alfvén and fast modes exists through 3-wave resonant interactions. In particular, it becomes strong at small  $\theta$  because the frequency of fast and Alfvén modes are comparable, which makes the interaction more efficient. This interaction tries to make the amount of fast mode comparable to Alfvén mode. The faster interaction of pure three-Alfvén mode and pure three-fast mode than the mixed interaction, however, prohibits the appearance of such a strong-coupling regime (Chandran 2005). On the other hand, Equation (27) shows that the relativistic correction term breaks such a complete decoupling of the velocity. We consider that this results in a stronger coupling.

The tendency of the fast to Alfvén mode velocity ratio increasing with  $\sigma$ -value in Figure 1 can be understood as follows. Assuming that only Alfvén mode exists in a plasma, it induces compressible modes because of its electromagnetic field pressure. The equation of motion along background magnetic field can be written as:

$$\partial_t [\rho h \delta v_{\parallel}] \simeq -\nabla (\delta B^2 + \delta E^2) / 2. \quad (31)$$

Using the eigen-mode relation of the Alfvén mode,  $(\delta E_A)^2 = (\delta v_A B_0)^2$  and  $(\delta B / B_0)^2 = (\delta v_A / c_A)^2$ , this reduces to

$$\left( \frac{\delta v_{\parallel}}{\delta v_A} \right) \sim (\sigma + 1/2) \left( \frac{\delta v_A}{c_A} \right), \quad (32)$$

where  $\omega = c_A k$  and  $B_0^2 / \rho h \simeq \sigma$  are used. This indicates that the higher the  $\sigma$ -value is, the more compressible modes are induced; On the other hand, it becomes independent of  $\sigma$ -value in the matter-energy dominated region,  $\sigma = 0$ , as indicated in (Cho & Lazarian 2002). The actual relation of fast and Alfvén modes also depends on the energy distribution between fast and slow mode, and on non-linear coupling of each modes, which will alter the  $\sigma$  dependence as indicated in Equation (28).

## 4.3 Energy Transfer Between Modes

Since in this work strong turbulence is considered, it is very difficult to explain the obtained numerical result thoroughly via an analytical method. Hence, in this section a series of numerical experiments were performed, and we discuss the mode conversion of each MHD mode in a Poynting-dominated plasma with  $\sigma = 5$ .

Figures 4 and 5 are temporal evolution of each mode velocity in the case of  $T = 0.1mc^2$  and  $T = 2.5mc^2$ , respectively. The total injected turbulent velocity dispersion is  $\delta v_{\text{inj}} = 0.45c_A$ . The top panels are the results when injecting only Alfvén mode turbulence. They show that the mode conversion from Alfvén mode to compressible modes is nearly independent of the background temperature, consistent with Figure 3. In both cases, the each mode energy density in the steady state is approximately described as:  $W_A : W_F : W_S \simeq 80 : 15 : 5$  in the  $\sigma = 5$  and isothermal plasma <sup>5</sup>.

<sup>5</sup> Note that in the vertical axes in Figures 4 and 5 the each mode power is renormalized by their total power  $\delta v^2$ . This is

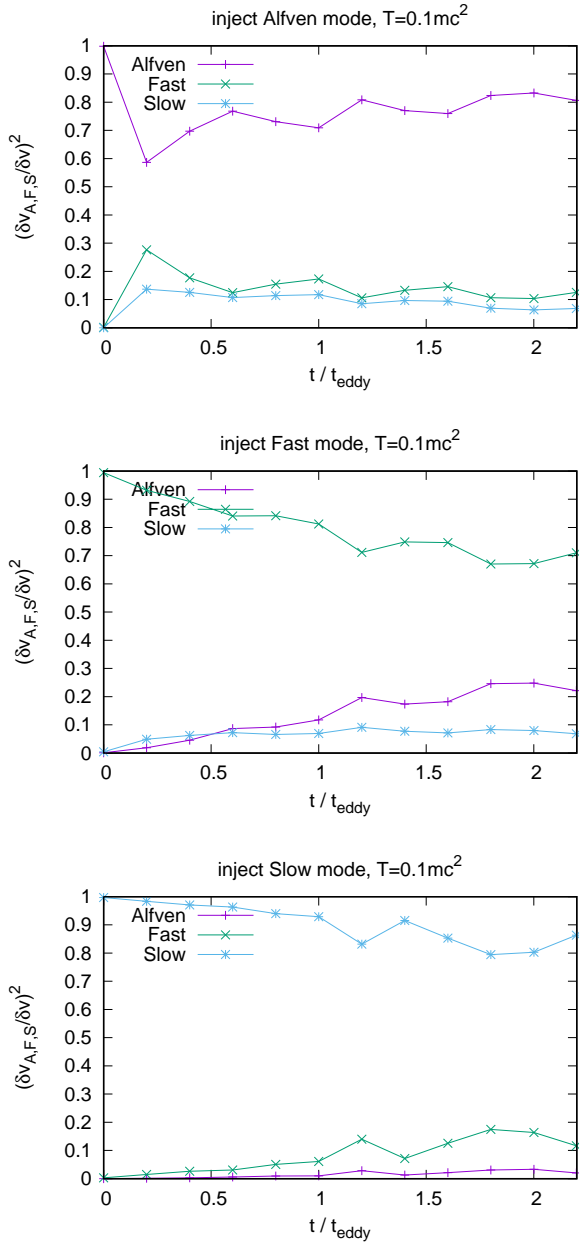


**Figure 4.** Temporal Evolution of each modes, in the case of  $\sigma = 5$  and  $T = 0.1mc^2$ . Top: only Alfvén mode is injected. Middle: only fast mode is injected. Bottom: only slow mode is injected.

The middle panels of Figures 4 and 5 are temporal evolution of each mode velocity when injecting only fast mode turbulence. They also show that the mode conversion from fast mode to the other modes is nearly independent of the background temperature. In both cases, the each mode energy in the steady state is approximately described as:  $W_A : W_F : W_S \simeq 20 : 70 : 10$ , indicating a stronger energy transfer between Alfvén and fast modes.

The bottom panels of Figures 4 and 5 are temporal evo-

the reason why the Alfvén mode looks like increasing after their sharp decrease at the initial phases. The Alfvén mode energy itself gradually decreases in time.

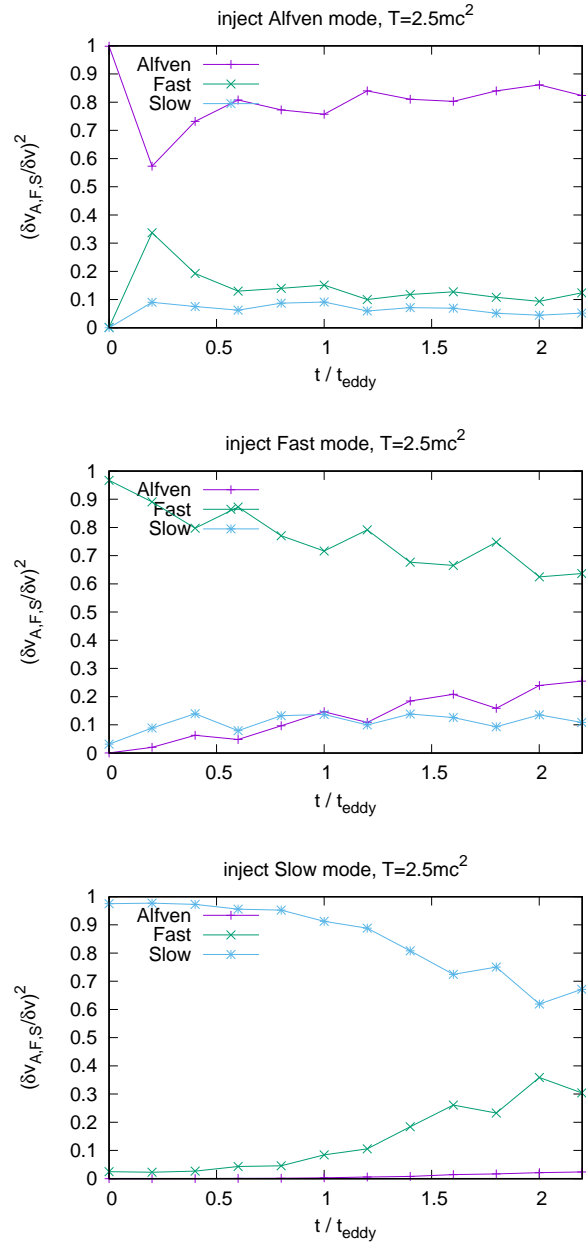


**Figure 5.** Temporal Evolution of each modes, in the case of  $\sigma = 5$  and  $T = 2.5mc^2$ . Top: only Alfvén mode is injected. Middle: only fast mode is injected. Bottom: only slow mode is injected.

lution of each mode velocity when injecting only slow mode turbulence. In contrast to the previous cases, they show a clear dependence of the slow to fast energy conversion on the background temperature. We consider that this may indicate the effect of the relativistic correction term in Equation (27) which induces a mixing of the velocity direction between fast and slow mode. Although it is very difficult to explain why slow to fast mode conversion seems much stronger than the opposite case due to the strong non-linearity in the turbulence, at least we found even in Figures 4 and 5 a slight increase of the mode conversion into slow mode can be observed. In Figure 4, the each mode energy in the steady state

is approximately described as:  $W_A : W_F : W_S \simeq 0 : 10 : 90$ , and in Figure 5,  $W_A : W_F : W_S \simeq 0 : 30 : 70$ .

Note that Figures 4 and 5 show that the initial Alfvén mode power is immediately transferred to the other modes, mainly into fast mode, much less than the eddy-turnover time which is the typical timescale of energy transfer in the case of the critical-balanced Alfvén mode turbulence. This is because in this regime the initial energy is not transferred by the mode-coupling but the pressure gradient force. The timescale of the energy conversion via the pressure gradient force can be estimated using Equation (31) as follows. In the case of the initial energy transfer, Equation (31) can be rewritten as:

$$\frac{\rho h \delta v_{\parallel}}{\tau_{\text{trans}}} \sim \frac{\delta B^2 + \delta E^2}{2L_{\text{inj}}}, \quad (33)$$

where  $L_{\text{inj}}$  is the initial injection scale, and  $\tau_{\text{trans}}$  is the energy transfer timescale. Assuming  $\delta v_{\parallel} \sim r_0 \delta v_{A,0}$ ,  $\delta B/B_0 \sim \delta v_{A,0}/c_A$ ,  $\delta E \sim \delta v_{A,0} B_0$ , the above equation reduces to:

$$\tau_{\text{trans}} \sim L_{\text{inj}} \frac{r_0}{\delta v_{A,0}^2} \frac{2}{2\sigma + 1}. \quad (34)$$

Note that  $\tau_{\text{trans}}$  describes the energy transfer timescale of the evolution of  $\delta v_{\parallel}$  from 0 to  $r_0 \delta v_{A,0}$  where  $\delta v_{A,0}$  is the initial Alfvén mode velocity and  $r_0$  is a constant coefficient. Substituting  $L_{\text{inj}} \sim L/3$ ,  $r_0 \sim 1$ , and  $\sigma = 5$ , the timescale becomes  $\tau_{\text{trans}}/(L/\delta v_{A,0}) \sim 0.06$ , which explains the initial rapid energy transfer described in Figures 4, 5, and 6.

#### 4.4 A Strong Coupling Regime

As we have seen in the previous sections, the obtained results indicate existing of a region where fast and Alfvén modes are strongly coupled, different from non-relativistic cases. From Figure 3, the coefficient  $A$  in Equation (28) is 0.33 in the case of isothermal plasma. Assuming  $\delta v_A/c_{f,\perp} = 0.5$ , the indicated  $\sigma$ -value necessary for this regime,  $\delta v_F \simeq \delta v_A$ , becomes  $\sigma = 35$ . Unfortunately, such a high- $\sigma$  plasma is very difficult to simulate by the present numerical simulation technique. Instead, we performed a run with a special initial condition that can temporally results in the strong regime, and studied its physical properties. The initial injected turbulence was composed by 80 % fast mode and 20 % Alfvén mode power, and the background plasma parameters are:  $\sigma = 5$  and  $T/mc^2 = 0.1$ . The total injected turbulent velocity dispersion is  $\delta v_{\text{inj}} = 0.45c_A$ . The other conditions were set the same as the other runs. The temporal evolution of each mode power is shown in the top-panel of Figure 6. It indicates that fast and Alfvén modes strongly couple around 1.5 eddy-turnover time. After that time, the coupling became weak, and the turbulence gradually evolved into a state indicated in Figure 3 because of insufficient background  $\sigma$ -value. In the following, we concentrate on the strong coupling regime appeared in this simulation. The bottom-panel of Figure 6 is the energy spectra of each velocity components at  $t = 1.6$  eddy-turnover time. First, it is found that strong fluctuations exist in the long wavelength region, and this makes it difficult to find a clear inertial region. In spite of this fact, it shows the energy spectra of fast and Alfvén modes clearly degenerates up to dissipation regime around  $k = 40$ ; This indicates that the strong coupling regime of the 2 mode was actually realized in this simulation. Its spectral index up

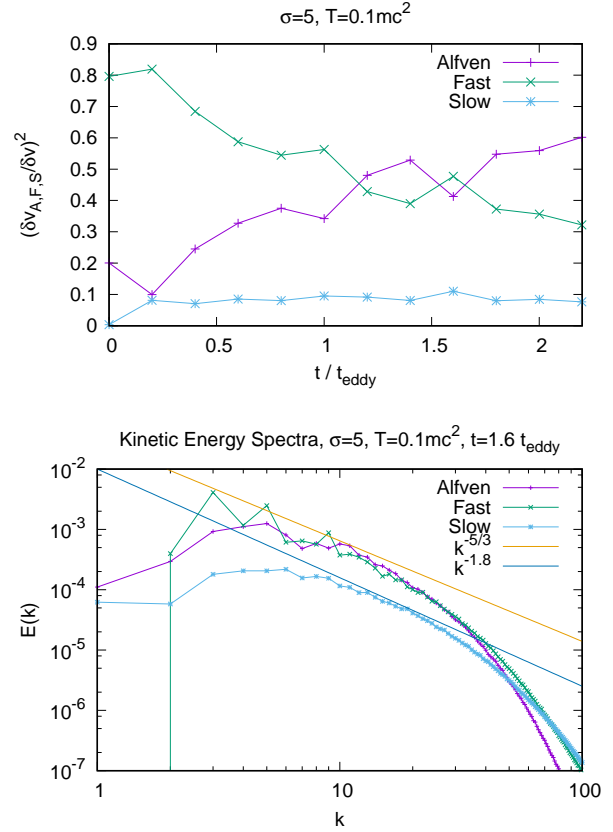


**Figure 6.** Top: Temporal Evolution of each modes when injecting  $(\delta v_A)^2 : (\delta v_F)^2 = 1 : 4$  in the case of  $\sigma = 5$  and  $T = 0.1mc^2$ . Bottom: kinetic energy spectra of each mode at  $t = 1.6t_{\text{eddy}}$ .

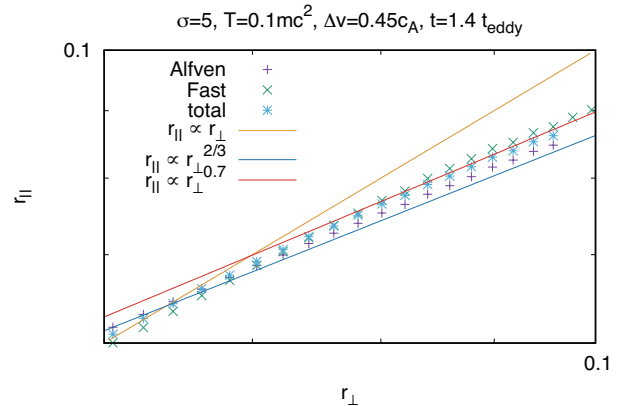


**Figure 7.** Eddy-shape of Alfvén and fast modes in the case of  $\sigma = 5$  and  $T = 0.1mc^2$  at  $t = 1.4t_{\text{eddy}}$ . The integrated case (no mode decomposition) is also plotted, which shows an intermediate region between isotropic:  $r_{\parallel} \propto r_{\perp}$  to critical balance case  $r_{\parallel} \propto r_{\perp}^{2/3}$ . The indicated power law index approximately 0.7.

to  $k = 20$  is approximately shallower than  $5/3$  but steeper than  $1.8$  which is observed in fast mode energy spectrum in our previous work TL16. However, the value of the index is clearly closer to  $5/3$  than  $1.8$ , and this indicates that the energy cascade into smaller scale length is mainly driven by Alfvén mode-like cascade process.

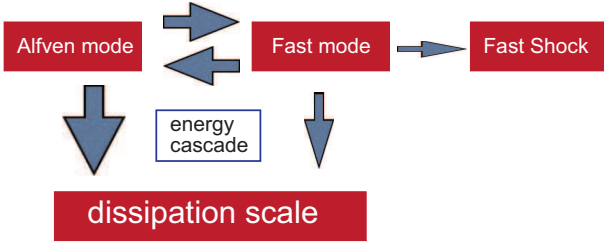


**Figure 8.** A schematic picture of the energy transfer in high- $\sigma$  turbulence.

Figure 7 shows the eddy-shape of the Alfvén, fast, and the total mode of the 2-modes. Following (Cho & Vishniac 2000), the eddy-shape is calculated from the 2nd-order structure function for the velocity. Note that the structure function is calculated in terms of the local magnetic field (Lazarian & Vishniac 1999; Cho & Vishniac 2000; Maron & Goldreich 2001), and the axes of the figure ( $r_{\perp}, r_{\parallel}$ ) means the radius of the eddy perpendicular and parallel to the local magnetic field. The figure shows that all the 3-lines can be described as:  $r_{\parallel} \propto r_{\perp}^{0.7}$  which is close to the critical balance law:  $r_{\parallel} \propto r_{\perp}^{2/3}$ . This also supports that the energy cascade is mainly governed by the Alfvén mode-like. This can be because the fast mode cascade is less efficient than the Alfvén mode cascade, and the strong coupling allows the fast mode energy to flow into Alfvén mode whose cascade is more efficient. The power law index is a little larger than the critical value  $2/3$ , and we consider that this correction is due to an effect of fast mode which usually shows isotropic eddy-shape  $r_{\parallel} \propto r_{\perp}$  as shown in TL16. Although the obtained results are just a state of temporally strong-coupling, we expect that it indicates the existence of the steady strong-coupling regime where a similar properties will be able to be observed.

## 5 DISCUSSION

Although it was impossible to show an existence of the strong-coupling regime due to the numerical difficulty of simulating strong turbulence in high- $\sigma$  plasma, we simulated a temporally strongly-coupling regime. In that regime, it is found that the energy spectra of Alfvén and fast modes are nearly the same whose spectral index is nearly  $5/3$ , possibly indicating the energy cascade is mainly via Alfvén mode-like cascade. We also studied the eddy shape in the strong-coupling regime. The obtained eddy shape is approximately  $r_{\parallel} \propto r_{\perp}^{0.7}$  which is slightly different from the shape indicated by the critical-balance,  $r_{\parallel} \propto r_{\perp}^{2/3}$ . We consider that this is due to the effect of the coupling to fast mode whose eddy shape is isotropic,  $r_{\parallel} \propto r_{\perp}$ . Although the obtained results are just a state of temporally strong-coupling, we expect that it indicates the existence of the steady strong-coupling regime where a similar properties will be able to be observed.

From these facts, one possible scenario can be proposed for the turbulence-energy transfer in the strong-coupling regime. The degeneration of the fast and Alfvén modes in Figures 7 and 8 indicates that the Alfvén and fast modes communicate with each other in large scale and inertial region, allowing energy transfer between the 2-modes; This

coupling, however, cannot be observed in the small scale region, or the dissipation region in Figure 7. This means that the energy dissipation process of Alfvén and fast modes are different. We consider that a possible candidate for the dissipation process of fast mode is the appearance of the fast-shock. It is well-known that the fast wave evolves into fast shock due to the non-linearity, and this allows to dissipate its own energy through shock dissipation as discussed in (Takamoto et al. 2014). Concerning the inertial regime, the eddy-shape and the spectral index of the energy spectrum indicate that the energy will be transferred mainly by the Alfvén mode-like cascade process, and a small amount of it by the fast mode-like cascade. In summary, it can be expected that there will be an energy cascade path of turbulence in high- $\sigma$  plasma as shown in Figure 8.

## 6 SUMMARY AND CONCLUSION

In this paper, we discussed a strong-coupling regime of Alfvén and fast modes of relativistic MHD turbulence in Poynting-dominated plasma. In our previous work TL16, we found an increase of the amount of the fast mode with background  $\sigma$ -value in the case of decaying turbulence in adiabatic plasma, which we consider as an indirect proof of strong-coupling between Alfvén and fast mode in sufficiently high- $\sigma$  plasma. It was, however, not clear if the increase of the amount of fast mode was affected by the increase of background temperature which reduces  $\sigma$ -value and may change the behavior of the mode exchange of RMHD turbulence. For this problem, in this work, isothermal plasma was considered that kept background plasma temperature constant. We found that the increase of the fast to Alfvén mode power ratio can be observed even in this case as shown in Figure 1. We consider that this is because the relativistic correction of the displacement vector of fast mode in high- $\sigma$  plasma which will encourage mixing of fast to the other two modes through 2nd-order interaction. We also performed a series of numerical studies of mode conversion. It showed that Alfvén mode turbulence actually generate fast mode turbulence in high- $\sigma$  plasma, and vice versa. In addition, we found that the mode exchange is nearly insensitive to the background temperature, other than the slow to fast mode conversion.

In conclusion, we found that the strong-coupling regime of Alfvén to fast modes was independent of the background temperature, and actually existed in high- $\sigma$  plasma turbulence. We emphasize that this alters the previous understanding on relativistic turbulence in high-energy astrophysical phenomena, which usually assumed either the non-relativistic critical balance or force-free limit. In this sense, our new findings will affect the understanding of particle acceleration and photon emission in high- $\sigma$  plasma turbulence, such as relativistic jets, pulsar wind nebulae, and gamma-ray bursts.

## ACKNOWLEDGMENTS

We would like to thank Sébastien Galtier, Supratik Banerjee, and Nobumitsu Yokoi for many fruitful comments and discussions. MT also would like to thank Tsuyoshi Inoue for

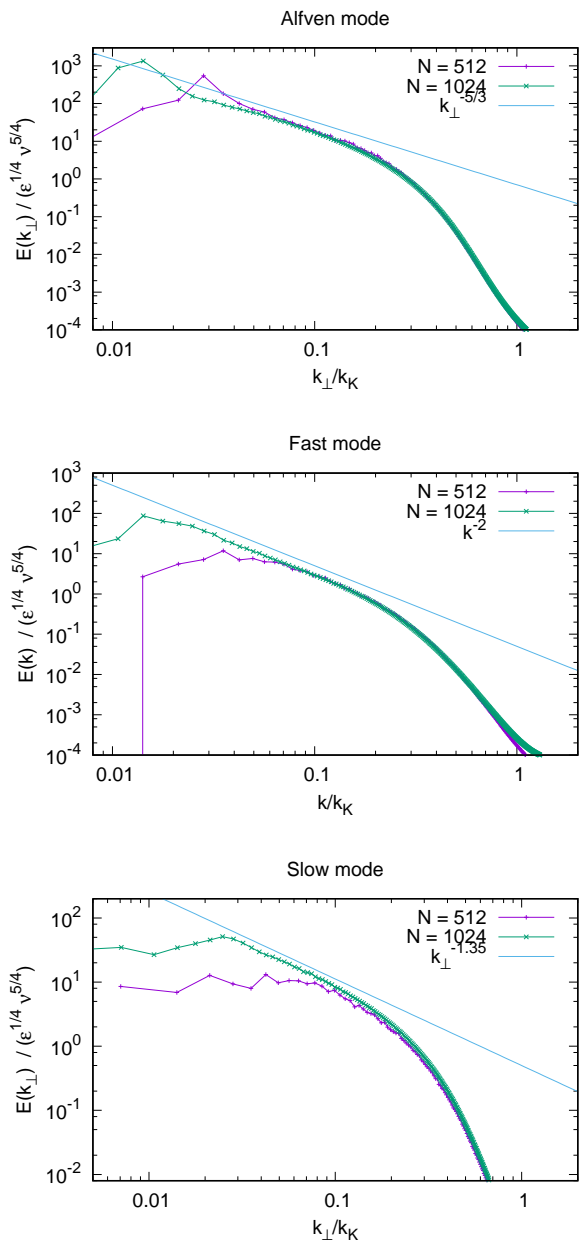


**Figure A1.** Non-dimensional energy spectra of each mode in driven turbulence in isothermal plasma with  $\sigma = 3$  and  $T/mc^2 = 0.1$ .

kindly providing with the original numerical code. Numerical computations were carried out on the Cray XC30 at Center for Computational Astrophysics, CfCA, of National Astronomical Observatory of Japan. This work is supported in part by the Postdoctoral Fellowships by the Japan Society for the Promotion of Science No. 201506571 (M. T.). AL is supported by NSF DMS 1622353.

## APPENDIX A: ENERGY SPECTRA OF DRIVEN TURBULENCE IN ISOTHERMAL PLASMAS

In this Appendix, we discuss energy spectra of each mode in high- $\sigma$  turbulence. In our previous work TL16, the numerical simulations of undriven turbulence in adiabatic plasma were performed, and the obtained energy spectra were discussed. On the other hand, in this work, so called *driven* turbulence is considered, which allows us to obtain turbulence without suffering from contamination by dissipation in its energy spectra. Note that we also consider an effect of cooling to avoid too much energy increase by injecting turbulence.

In this work, turbulence is injected by adding to momentum flux density,  $\rho h \gamma^2 \delta \mathbf{v}$ , where  $\delta \mathbf{v}$  is a turbulent velocity obtained the same method as described in Section 2. The background plasma parameters are  $\sigma = 3$  and  $T/mc^2 = 0.1$ . The strength of the injected turbulence is  $|\delta v| = 0.5c_A$ . The turbulence is injected at every fixed timestep,  $dt_{\text{inj}} = \sqrt{2}t_{\text{eddy}}/10$ <sup>6</sup>.

The main purpose of this section is to discuss properties of inertial region of each mode. Unfortunately, it is usually very difficult to find clear inertial region of relativistic MHD turbulence because of insufficient numerical resolutions. To avoid such a problem, a new strategy is proposed by (Beresnyak 2014; Beresnyak & Lazarian 2015), which uses the self-similar property of turbulence, so-called *Kolmogorov's similarity law* (Kolmogorov 1941), originally formulated in the case of pure hydrodynamic turbulence. This theory predicts that the energy spectrum of scale-invariant turbulence should be described as:

$$E(k) = \nu^{5/4} \epsilon^{1/4} e(k/k_K), \quad (\text{A1})$$

where  $\nu$  is kinetic viscosity,  $\epsilon$  is the energy cascade rate,  $e(k)$  is a non-dimensional power-law distribution function, and

$$k_K \equiv \left(\frac{\epsilon}{\nu}\right)^{1/4}, \quad (\text{A2})$$

is the Kolmogorov wavenumber describing a characteristic length of dissipation. This tells that the non-dimensional energy spectrum,  $e(k/k_K) = E(k/k_K)/(\nu^{5/4} \epsilon^{1/4})$ , should be independent of the background Reynolds number, and a clear inertial region can be found by comparing the simulation results with different resolution or Reynolds number.

Figure A1 is the obtained non-dimensional energy spectra of each mode at  $t = 2t_{\text{eddy}}$  when the turbulence reached a steady state<sup>7</sup>. We assumed that  $\nu$  can be written as  $\nu = Cc_s \Delta x$  where  $\Delta x$  is the mesh size, and  $C$  is a constant value describing numerical dissipation in our simulation<sup>8</sup>. They indicate that the relativistic MHD turbulence in high- $\sigma$  plasma follows the Kolmogorov's similarity law. The obtained energy spectra in the inertial region can be read approximately as  $-5/3$ ,  $-2$ ,  $-1.35$  in the case of Alfvén, fast, and slow modes, respectively. The value of the index of Alfvén mode,  $-5/3$ , is consistent with our previous work

<sup>6</sup> We saved data at every  $0.2t_{\text{eddy}}$ . The factor  $\sqrt{2}$  is added to avoid injecting turbulence at the same time step of data saving.

<sup>7</sup> The energy spectra were obtained using a framework for parallel computations of Fourier transforms in three dimensions (Pekurovsky 2012).

<sup>8</sup> For the value of  $C$ , we took unity when  $N = 512$  and 0.8 when  $N = 1024$ .

TL16. Interestingly, the fast mode becomes much steeper than that of decaying turbulence, -1.86, obtained in TL16. On the other hand, the slow mode shows a very shallow spectrum, -1.35, although TL16 cannot have found a clear inertial region of slow mode turbulence. It is still unclear that the observed spectra suffered the injection scale or not, though it seems not affected from dissipation scale. And it is necessary to perform much larger simulation in the future in order to obtain a robust conclusion.

Finally, in this simulation, sub-Alfvénic turbulence is injected, and this induces a mixed regime of weak and strong turbulence in long and short wave length regime (Lazarian & Vishniac 1999). In Figure A1, however, we cannot find a weak regime characterized by the spectral index -2. We consider that this is due to the resolution used in this simulation. The transition from weak to strong turbulence was first observed in (Meyrand et al. 2016), which used more than 3000 meshed in the direction perpendicular to the background magnetic field. In addition, we considered a magnetically-dominated plasma, which demands, in general, higher resolution to resolve the energy cascade in the perpendicular direction.

## REFERENCES

- Anile A. M., 1990, *Relativistic Fluids and Magneto-fluids*  
 Antón L., Miralles J. A., Martí J. M., Ibáñez J. M., Aloy M. A., Mimica P., 2010, *ApJS*, 188, 1  
 Balsara D., 2001, *ApJS*, 132, 83  
 Beresnyak A., 2014, *ApJL*, 784, L20  
 Beresnyak A., Lazarian A., 2015, in Lazarian A., de Gouveia Dal Pino E. M., Melioli C., eds, *Magnetic Fields in Diffuse Media Vol. 407 of Astrophysics and Space Science Library, MHD Turbulence, Turbulent Dynamo and Applications*. p. 163  
 Chandran B. D. G., 2005, *Physical Review Letters*, 95, 265004  
 Cho J., 2005, *ApJ*, 621, 324  
 Cho J., Lazarian A., 2002, *Physical Review Letters*, 88, 245001  
 Cho J., Lazarian A., 2003, *MNRAS*, 345, 325  
 Cho J., Lazarian A., 2014, *ApJ*, 780, 30  
 Cho J., Lazarian A., Vishniac E. T., 2002, *ApJ*, 564, 291  
 Cho J., Vishniac E. T., 2000, *ApJ*, 539, 273  
 Evans C. R., Hawley J. F., 1988, *ApJ*, 332, 659  
 Gardiner T. A., Stone J. M., 2005, *Journal of Computational Physics*, 205, 509  
 Goldreich P., Sridhar S., 1995, *ApJ*, 438, 763  
 Inoue T., Asano K., Ioka K., 2011, *ApJ*, 734, 77  
 Kolmogorov A., 1941, *Akademiia Nauk SSSR Doklady*, 30, 301  
 Komissarov S. S., 1999, *MNRAS*, 303, 343  
 Kuznetsov E. A., 2001, *Soviet Journal of Experimental and Theoretical Physics*, 93, 1052  
 Lazarian A., Vishniac E. T., 1999, *ApJ*, 517, 700  
 Maron J., Goldreich P., 2001, *ApJ*, 554, 1175  
 Meyrand R., Galtier S., Kiyani K. H., 2016, *Physical Review Letters*, 116, 105002  
 Mignone A., Plewa T., Bodo G., 2005, *ApJS*, 160, 199  
 Mignone A., Ugliano M., Bodo G., 2009, *MNRAS*, 393, 1141  
 Pekurovsky D., 2012, *SIAM Journal on Scientific Computing*, 34, C192  
 Radice D., Rezzolla L., 2013, *ApJL*, 766, L10  
 Synge J. L., 1957, *The relativistic gas*. Vol. 32, North-Holland Amsterdam  
 Takamoto M., Inoue T., Lazarian A., 2015, *ApJ*, 815, 16  
 Takamoto M., Kisaka S., Suzuki T. K., Terasawa T., 2014, *ApJ*, 787, 84  
 Takamoto M., Lazarian A., 2016, *ApJL*, 831, L11  
 Thompson C., Blaes O., 1998, *PRD*, 57, 3219  
 Zrake J., MacFadyen A. I., 2012, *ApJ*, 744, 32  
 Zrake J., MacFadyen A. I., 2013, *ApJL*, 763, L12

This paper has been typeset from a  $\text{\TeX}$ / $\text{\LaTeX}$  file prepared by the author.